Evolution of central dark matter of early-type galaxies up to $z \sim 0.8$

C. Tortora,[1]★ N. R. Napolitano,[1] R. P. Saglia,[2,3] A. J. Romanowsky,[4,5] G. Covone[6,7] and M. Capaccioli[6,7]

[1]*INAF – Osservatorio Astronomico di Capodimonte, Salita Moiariello, 16, I-80131 Napoli, Italy*
[2]*Max-Planck-Institut für extraterrestrische Physik, Giessenbachstrasse, D-85748 Garching, Germany*
[3]*Universitäts-Sternwarte München, Scheinerstrasse 1, D-81679 München, Germany*
[4]*Department of Physics and Astronomy, San José State University, San Jose, CA 95192, USA*
[5]*University of California Observatories, 1156 High Street, Santa Cruz, CA 95064, USA*
[6]*Dipartimento di Scienze Fisiche, Università di Napoli Federico II, Compl. Univ. Monte S. Angelo, I-80126 Napoli, Italy*
[7]*INFN Sez. di Napoli, Compl. Univ. Monte S. Angelo, Via Cinthia, I-80126 Napoli, Italy*

ABSTRACT

We investigate the evolution of dark and luminous matter in the central regions of early-type galaxies up to $z \sim 0.8$. We use a spectroscopically selected sample of 154 cluster and field galaxies from the ESO Distant Clusters Survey (EDisCS), covering a wide range in redshifts ($z \sim 0.4$–0.8), stellar masses ($\log M_\star/M_\odot \sim 10.5$–11.5 dex) and velocity dispersions ($\sigma_\star \sim 100$–300 km s^{-1}). We obtain central dark matter (DM) fractions by determining the dynamical masses from Jeans modelling of galaxy aperture velocity dispersions and the $M_\star$ from galaxy colours, and compare the results with local samples. We discuss how the correlations of central DM with galaxy size (i.e. the effective radius, R_e), $M_\star$ and $\sigma_\star$ evolve as a function of redshift, finding clear indications that local galaxies are, on average, more DM dominated than their counterparts at larger redshift. This DM fraction evolution with z can be only partially interpreted as a consequence of the size–redshift evolution. We discuss our results within galaxy formation scenarios, and conclude that the growth in size and DM content which we measure within the last 7 Gyr is incompatible with passive evolution, while it is well reproduced in the multiple minor merger scenario. We also discuss the impact of the initial mass function (IMF) on our DM inferences and argue that this can be non-universal with the look-back time. In particular, we find that the Salpeter IMF can be better accommodated by low-redshift systems, while producing stellar masses at high z which are unphysically larger than the estimated dynamical masses (particularly for lower $\sigma_\star$ systems).

Key words: galaxies: elliptical and lenticular, cD – galaxies: evolution – galaxies: general.

1 INTRODUCTION

Dark matter (DM) is a ubiquitous component of the universe. It dominates the mass density of virialized objects and has left its imprint at cosmological scales during the cosmic history (e.g. Komatsu et al. 2011). In the last decade, the large wealth of data from large sky surveys such as the Sloan Digital Sky Survey (SDSS; Abazajian et al. 2003, 2009; Adelman-McCarthy et al. 2008) have established that the DM budget is up to ∼85 per cent of the total mass density of the universe. Numerical simulations of (DM only) structure formation within the consensus cosmology framework, i.e. the Λ cold

dark matter (ΛCDM) model, have provided accurate predictions on the DM density distribution in galaxies and clusters (Navarro, Frenk & White 1996, hereafter NFW; Bullock et al. 2001; Macciò, Dutton & van den Bosch 2008). More realistic models, which have tried to evaluate the effect of baryons on the DM distribution, have been characterized either through some approximate recipes such as the adiabatic contraction (e.g. Gnedin et al. 2004), which seems compatible with observations (e.g. Gnedin et al. 2007; Napolitano, Romanowsky & Tortora 2010), or to the simultaneous evolutions of the two components (Wu et al. 2014), making predictions on the expected DM fractions in the central galaxy regions (Hilz, Naab & Ostriker 2013).

Within this context, the study of the mass density distribution and the dark-to-baryonic mass ratio of early-type galaxies (ETGs,

★ E-mail: ctortora@na.astro.it

ellipticals and lenticulars) is a crucial problem that has to be addressed in a systematic way, as these systems contain most of the cosmic stellar mass of the universe and represent the final stage of galaxy evolution, and contain the fossil record of the stellar and DM assembly through time.

Most of the current understanding of these systems is based on local galaxy samples. These have shown that the overall DM content depends crucially on the galaxy mass scale, which is possibly the effect of the overall star formation efficiency (Benson et al. 2000; Marinoni & Hudson 2002; Napolitano et al. 2005; Mandelbaum et al. 2006; van den Bosch et al. 2007; Conroy & Wechsler 2009; Moster et al. 2010). DM has been found to be relevant in the central galaxy regions (Gerhard et al. 2001; Padmanabhan et al. 2004; Cappellari et al. 2006; Thomas et al. 2007, 2009, 2011; Cardone et al. 2009, 2011; Hyde & Bernardi 2009; Tortora et al. 2009, T+09 hereafter; Auger et al. 2010; Cardone & Tortora 2010; Tortora et al. 2012) where ETGs show a substantial consistency with the concordance ΛCDM scenario (Napolitano et al. 2010; Tortora et al. 2012) and also some new scaling relations, like the one between DM fraction and formation epoch (Napolitano et al. 2010; Tortora et al. 2010b), which still need to be confirmed and fully understood.

Generally speaking, it has been shown that the central DM fraction (typically within one effective radius, R_e hereafter) is larger in more massive and large-sized galaxies (e.g. Hyde & Bernardi 2009; Ruszkowski & Springel 2009; T+09; Auger et al. 2010; Napolitano et al. 2010; Thomas et al. 2011; Tortora et al. 2012), even though there are also opposite claims from other studies (e.g. Grillo et al. 2009; Grillo 2010; Grillo & Gobat 2010). Although these trends are qualitatively unchanged independently of the adopted galaxy model or initial mass function, IMF (e.g. Cardone et al. 2009, 2011; Cardone & Tortora 2010), they can still be strongly affected by the assumptions on the stellar M/L, i.e. a non-homologous constant profile, as verified for the trend of the DM fraction as a function of mass (e.g. Trujillo, Burkert & Bell 2004; T+09; Tortora et al. 2012). The inventory of the pieces of evidence accumulated so far is complicated if one takes into account the effect of a non-universal IMF (Treu et al. 2010; Thomas et al. 2011; Cappellari et al. 2012, 2013b; Conroy & van Dokkum 2012; Spiniello et al. 2012; Wegner et al. 2012; Dutton et al. 2013; Ferreras et al. 2013; Goudfrooij & Kruijssen 2013; La Barbera et al. 2013; Tortora, Romanowsky & Napolitano 2013; Weidner et al. 2013; Goudfrooij & Kruijssen 2014; Tortora et al. 2014), which remains the largest source of uncertainty, since a systematic variation of the IMF with mass, from a bottom-lighter IMF for low-mass systems to a bottom-heavier IMF in massive galaxies, would wipe out the 'apparent' DM fraction trend with mass (e.g. Thomas et al. 2011; Tortora et al. 2013).

A robust assessment of all these correlations is crucial to have a clearer insight into the assembly of the two main galaxy components (stars and DM), and thus into the formation mechanisms across time. Unfortunately, with the currently available individual data sets, which generally cover small windows in redshift space, it is not possible to extend the investigation of the scaling relations found at lower z to earlier epochs (but see, for instance, Auger et al. 2009, 2010; Tortora et al. 2010b; Sonnenfeld et al. 2013 for gravitational lenses). Only by accumulating data from different samples, a more systematic study of the DM fraction evolution with redshift is becoming possible.

This has been done, e.g., using weak and/or strong lensing analyses (e.g. Heymans et al. 2006; Lagattuta et al. 2010) to find that at higher redshift results point to an evolution of the total virial-to-stellar ratio that is larger at higher redshift. For the central DM content, results are still inconclusive, as both lower DM fractions

(Faure et al. 2011, within the Einstein radius) and larger ones (Ruff et al. 2011, within $R_e/2$) have been found. However, the latter studies are based on limited galaxy samples with different model choices (e.g. on adopted scales at which the DM fractions are derived); thus, their conclusions are prone to uncertainties which are difficult to keep under control.

Instead, homogeneous approaches on well-studied high-z samples are still missing. Only recently, using massive galaxies from SDSS-III's Baryon Oscillation Spectroscopic Survey (SDSS-III/BOSS) combined with a sample from SDSS-II, Beifiori et al. (2014) have addressed the question, providing evidence that high-z ETGs are less DM dominated than their local counterparts. However, further independent analyses are needed to constrain not only the overall evolution of central DM, but also how it correlates with mass or galaxy size, and how these correlations change as a function of redshift.

The EDisCS sample (White et al. 2005; Saglia et al. 2010) includes ETGs in a wide range of redshifts (∼0.4–0.8) for which accurate photometry, structural parameters and central velocity dispersions are available. This provides us a rare opportunity to investigate the evolution of the central DM content, comparing these results with inferences in local galaxy samples.

The paper is organized as follows. Data samples and the analysis performed are introduced in Section 2. The evolution of the relations between size and velocity dispersion with stellar mass is discussed in Section 3, while Section 4 is devoted to the analysis of central DM content, its evolution with redshift, systematics and the interpretation within the formation scenarios. Conclusions and future prospects are discussed in Section 5. We adopt a cosmological model with $(\Omega_m, \Omega_\Lambda, h) = (0.3, 0.7, 0.75)$, where $h = H_0/100 \, \mathrm{km \, s^{-1} \, Mpc^{-1}}$ (Komatsu et al. 2011).

2 SAMPLES AND DATA ANALYSIS

The aim of this paper is to present a uniform dynamical analysis for galaxies distributed on a wide redshift window. As higher redshift galaxies, we will use the sample from EDisCS survey (Saglia et al. 2010), which covers a redshift window from $z \sim 0.4$ to $z \sim 0.8$. As $z \sim 0$ comparison samples, we use the data from the SPIDER project (La Barbera et al. 2010), ATLAS³D (Cappellari et al. 2011) and from T+09. In the following, we will provide further details about data samples adopted.

2.1 EDisCS sample: data

The EDisCS survey (White et al. 2005; Saglia et al. 2010) provides photometric and spectroscopic data for ETGs in field and rich clusters with $0.4 \lesssim z \lesssim 0.8$ and stellar mass completeness limit at $\log M_\star/M_\odot = 10.4$. We limit the analysis to objects with spectroscopic measurements, as these provide us accurate redshifts and internal kinematics. The final sample which we will use for this analysis has been further selected to have weak [O II] lines in order to remove late-type galaxies and contains 41 field galaxies and 113 in clusters.

For these systems, circularized *Hubble Space Telescope I*-band effective radii, R_e, and Sérsic fitting indices, n, are available.

The average slit width of the spectral observations, from which velocity dispersions have been derived, has been converted to an equivalent circular aperture of radius $\approx 1.025 \, (\delta x/\pi)$, where δx is the slit width, in arcsec. The ratio between spectral aperture and the effective radius, R_{ap}/R_e, amounts to ∼1.5, with a tail to higher ratios.

As reference stellar masses, we have taken the ones from Saglia et al. ([2010](#)), using rest-frame absolute photometry derived from spectral energy distribution (SED) fitting (Rudnick et al. [2009](#)), adopting the calibrations of Bell & de Jong ([2001](#)), with a 'diet' Salpeter IMF and $B − V$ colours. These masses are renormalized to a Chabrier IMF subtracting ∼0.1 dex, accordingly to results in T+09. Our masses are in very good agreement with those in Vulcani et al. ([2011](#)).

2.2 High-z sample: dynamics of EDisCS galaxies

Following the analysis in T+09 and Tortora et al. ([2012](#)), we model the velocity dispersion of each individual galaxy using the spherical isotropic Jeans equations, and hence estimate the (total) dynamical mass M_{dyn} (which, hereafter, we will refer to as M_{tot}) within $r = 1\,R_e$.

In the Jeans equations, the stellar density is provided by the Sérsic fit of the photometric data, and the total (DM + stars) mass is assumed to have the form of a singular isothermal sphere (SIS), from which $M(r) \propto \sigma_{SIS}^2 r$, where σ_{SIS} is the model (3D) velocity dispersion.

The isothermal profile has been found to provide a robust description of the mass distribution in massive ETGs (e.g. Kochanek [1991](#); Bolton et al. [2006](#), [2008](#); Koopmans et al. [2006](#); Gavazzi et al. [2007](#); Auger et al. [2009](#), [2010](#); Chae, Bernardi & Kravtsov [2014](#); Oguri, Rusu & Falco [2014](#)), and in particular the massive dark haloes dominating the outer regions of galaxies (Benson et al. [2000](#); Marinoni & Hudson [2002](#); Napolitano et al. [2005](#); Gavazzi et al. [2007](#); van den Bosch et al. [2007](#)). This 'conspiracy' (Rusin, Kochanek & Keeton [2003](#); Treu & Koopmans [2004](#); Koopmans et al. [2006](#); Gavazzi et al. [2007](#); Auger et al. [2010](#)) seems to be motivated also by theoretical arguments as the stellar body and dark haloes can produce an overall isothermal profile after having gone through the processes of gas contraction and star formation (Koopmans et al. [2006](#); Remus et al. [2013](#)). For further details on the systematics introduced by the particular model choice, one can refer to T+09 and Tortora et al. ([2012](#), see also Cardone et al. [2009](#), [2011](#); Cardone & Tortora [2010](#)). However, in Section 4.1.2, we will discuss the impact on our results of the slope of the galaxy model adopted.

2.3 Reference $z \sim 0$ samples

We use three local data sets of ETGs to compare with high-z results. For these samples, we have performed the same dynamical analysis and use similar assumptions for the stellar and total density profiles as the ones for the high-z sample discussed in Section 2.2. Here below are given some details of the local data sets.

(i) *SPIDER.* This is the widest local data sample analysed in this paper, consisting of ∼4300 giant ETGs in the redshift range of $z = 0.05$–0.1 (La Barbera et al. [2010](#)). The data set includes optical+near-infrared photometry (from the SDSS and the United Kingdom Infrared Telescope (UKIRT) Infrared Deep Sky Survey-Large Area Survey), high-quality measurements of galactic structural parameters (effective radius R_e and Sérsic index n) and SDSS central aperture velocity dispersions σ_{Ap}. The sample galaxies are defined as bulge-dominated systems with passive spectra while late-type systems are removed through the SDSS classification parameters based on the spectral type and the fraction of light which is better described by a de Vaucouleurs ([1948](#)) profile (see Tortora et al. [2012](#) for further details). The sample is 95 per cent complete at the stellar mass $M_\star = 3 \times 10^{10}\,M_\odot$, which corresponds

to $\sigma_{Ap} \sim 160\ \mathrm{km\,s^{-1}}$. The stellar population synthesis (SPS)-based stellar mass-to-light ratios, $\Upsilon_\star$, were derived by fitting Bruzual & Charlot ([2003](#)) models to the multiband photometry, assuming a Chabrier IMF [see Swindle et al. ([2011](#)) and Tortora et al. ([2012](#)) for further details]. A de-projected Sérsic law in the K band is used to describe the density profile of the stellar component. Then, both the light profile and total masses are calculated at g-band R_e, whose rest frame is approximately the observed I band from EDisCS. The trends at $R_{e,K}$ will be discussed too.

(ii) *T+09.* This data set contains optical photometry and kinematics of the galaxy central regions from Prugniel & Simien ([1996](#)). The colours are measured within 1 R_e; the central velocity dispersions σ_0 are measured in circular aperture of radius $R_e/8$ from long-slit spectra. Non-homology in the light profile is taken into account using the n–L_B correlation in Prugniel & Simien ([1997](#)). V_{max} is defined as the quadratic sum of the maximum rotation on the major and minor axes, and is taken into account in the dynamical modelling. Selecting galaxies with at least two measured colours brighter than $M_B = −16$ and further limiting the sample to ellipticals and lenticulars, we are left with ∼360. See T+09 for further details on the sample selection and analysis. The B band, like the g band, approximates very well the rest frame of I-band measurements in EDisCS galaxies.

(iii) *ATLAS*^{3D}. This sample is originally constituted of 260 ETGs from the ATLAS^{3D} survey (Cappellari et al. [2013a](#),[b](#)). About 15 per cent of the sample have significant gradients of the stellar mass-to-light ratio, as inferred by their young stellar populations (Hβ equivalent width greater than 2.3 Å). We exclude these systems and retain a sample of 224 galaxies. The relevant data for each galaxy include the effective radius, R_e (obtained by renormalizing their R_e from multi-gaussian expansion (MGE) light profiles with a factor of 1.35), the projected stellar velocity dispersion, σ_e, within a circularized aperture of radius R_e, the r-band total luminosity L_r and stellar M/L ($\Upsilon_\star$) derived by SPS fitting of the spectra with Vazdekis et al. ([2012](#)) models and a Salpeter ([1955](#)) IMF. The Chabrier ([2001](#)) IMF yields stellar masses that are ∼0.26 dex smaller (see also Tortora et al. [2014](#) for further details).

These three local samples allow us to evaluate the impact on the results of (a) the prescription for light distribution profiles, (b) the apertures used to measure velocity dispersion and (c) SPS prescriptions for stellar mass estimates. As we will see, the trends are nearly independent of the sample adopted, making the results quite robust.

3 SIZE–MASS AND FABER–JACKSON EVOLUTION

A simple monolithic-like scenario, where the bulk of the stars are formed in a single dissipative event followed by a passive evolution, is no longer supported by the observations, while it is becoming increasingly evident in the occurrence of a strong mass and size evolution in ETGs (Trujillo et al. [2006](#); Trujillo, Ferreras & de La Rosa [2011](#)).

For the analysis we want to perform, we are interested in comparing some relevant correlations found in local galaxies, such as the ones between the galaxy size, i.e. R_e, and the stellar mass, $M_\star$, and the one between the velocity dispersion and $M_\star$ (see e.g. T+09; La Barbera et al. [2010](#); Cappellari et al. [2013a](#)) with the same for high-z galaxies (Saglia et al. [2010](#)).

In Fig. [1](#), we show the R_e–$M_\star$ relation for each galaxy of the four samples colourized according to their central velocity dispersion.
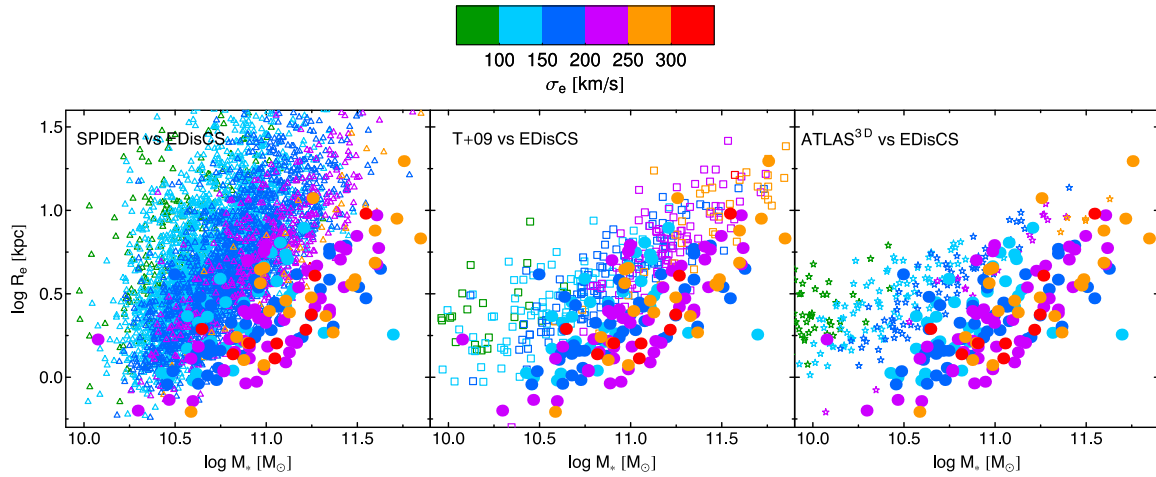
Figure 1. Size–mass relation colourized according to the σ_e bins in the colour bar (grayscale bar in the B&W version) in the top. We show single data points for single galaxies: *I*-band EDisCS (points), *g*-band SPIDER (open triangles), *B*-band T+09 (open squares) and *r*-band ATLAS^{3D} (open stars).
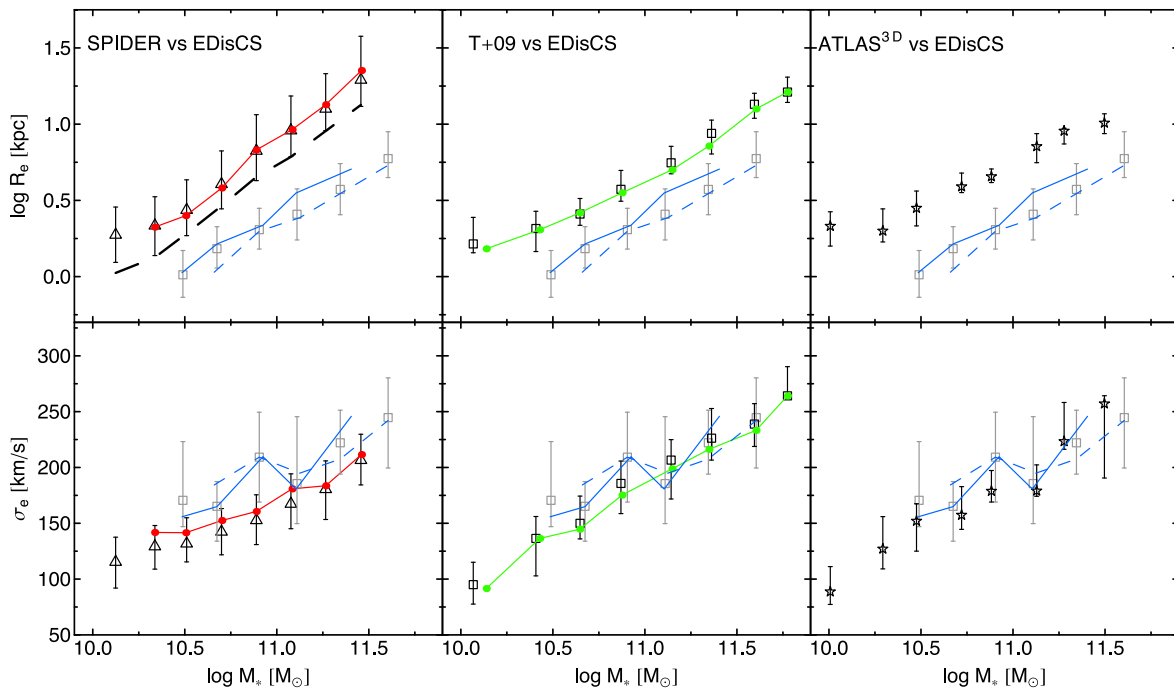

Figure 2. Size–mass (top panels) and σ_e–mass (bottom panels) relations. Medians and 25–75th quantiles are plotted. The EDisCS sample is plotted as grey symbols; *I*-band R_e are used. The average trends for lower z (z ≤ 0.6, blue lines) and higher z (z > 0.6, blue dashed lines) EDisCS galaxies are also plotted. See the text for further details about bin selection. From left to right, we compare EDisCS results with *g* band (open triangles) and *K* band (dashed line) from SPIDER, *B* band from T+09 (open squares) and *r* band from ATLAS^{3D} survey (open stars). Red (green) points and lines are for results corrected for progenitor bias for SPIDER (T+09) data sets.

This figure provides insights into the covariance among the stellar and dynamical parameters relevant in our analysis; we will adopt a similar approach in the next section when we will discuss the central DM content. Both low- and high-z galaxies follow the typical positive R_e–$M_\star$ relation. It is also evident that a similar positive correlation exists between σ_e and $M_\star$, independently of the redshift, as higher σ_e galaxies are more concentrated at the higher stellar masses and lower σ_e are found towards lower stellar masses both for high-z and the low-z samples. This is made clearer in Fig. 2, where we show the median results of the EDisCS sample compared

face-to-face to the three local samples. The correlations for each data sample are quantified with a log–log fit, and the best-fitting parameters are reported in Table 1.

Consistently with the local observations and independently of differences in the bands adopted for the R_es, the EDisCS sample presents the same size–mass trend, with more massive galaxies being larger (top panels in Fig. 2 and Table 1). All the correlations are significant at more than 99 per cent. Moreover, at fixed mass, the high-z galaxies in the EDisCS sample show a systematic offset towards smaller radii with respect to the same quantities for the

Table 1. Best-fitting parameters for the relation $\log R_{\rm e} = a + b \log \left(M_\star/10^{11} \right)$ and $\log \sigma_{\rm e} = a + b \log \left(M_\star/10^{11} \right)$ for the samples analysed. Best value, 1σ error and significance of the correlation are shown.

Sample	$R_{\rm e}$–$M_\star$			$\sigma_{\rm e}$–$M_\star$		
	a	b	Significance	a	b	Significance
SPIDER	0.89 ± 0.01	0.81 ± 0.04	99 per cent	2.212 ± 0.004	0.18 ± 0.02	99 per cent
T+09	0.69 ± 0.01	0.58 ± 0.03	99 per cent	2.265 ± 0.007	0.27 ± 0.01	99 per cent
ATLAS[3D]	0.75 ± 0.02	0.50 ± 0.04	99 per cent	2.28 ± 0.01	0.29 ± 0.02	99 per cent
EDisCS	0.35 ± 0.03	0.61 ± 0.08	99 per cent	2.29 ± 0.02	0.15 ± 0.04	99 per cent
EDisCS – low z	0.42 ± 0.05	0.69 ± 0.12	99 per cent	2.29 ± 0.03	0.19 ± 0.06	99 per cent
EDisCS – high z	0.31 ± 0.04	0.66 ± 0.10	99 per cent	2.3 ± 0.02	0.11 ± 0.06	99 per cent

local samples, i.e. they are more compact at all masses. The same is found for the Sérsic indices (not shown) which are smaller than the local values. Instead, the slope of the size–mass for the EDisCS sample is identical to the ones of most of the samples analysed and a bit shallower than SPIDER sample.[1] The high-z galaxies are, on average, ~ 2–4 times smaller than local SPIDER galaxies while only ~ 2 smaller than the other local samples (T+09 and ATLAS[3D]). If K-band $R_{\rm e}$s are used for SPIDER galaxies, then the difference with respect to the high-z sample becomes more similar to that found for the other local samples.

We have also split the high-z sample in two further bins to see whether there is the signature of a further evolution with z within the EDiSC sample itself. The two subsamples are selected to have redshifts ≤ 0.6 and > 0.6, and have median redshifts of 0.52 and 0.75, respectively. We find that the trends are almost unchanged (see Table 1) and that there is possibly a further evolution in the intrinsic size towards more compact $R_{\rm e}$ at higher z (Saglia et al. 2010).

Going to the correlations between velocity dispersion and stellar mass, this is also seen in the EDisCS sample (bottom panels in Fig. 2 and Table 1). At fixed stellar mass, no significant evidence of evolution is found with respect to the local samples, except a marginal offset at $M_\star \lesssim 10^{11} \, {\rm M}_\odot$, which shows smaller $\sigma_{\rm e}$ than the ones in EDisCS. In this case, the spitting of the EDisCS into two z bins does not show any further evolution signatures (see Fig. 2 and Table 1).

This mild evolution in velocity dispersion is consistent with predictions from galaxy mergers (Cenarro & Trujillo 2009; Hopkins et al. 2009), but not with the puffing-up scenario in Fan et al. (2008), which would produce a stronger change with redshift.

The results shown in Figs 1 and 2 do not take into account the progenitor bias, for which low-z ETG samples contain galaxies that have stopped their star formation only recently and that would not be recognized as ETGs at higher redshifts. In particular, a morphologically selected local sample of ETGs as the ones we have analysed contains systems with relatively young ages that, when evolved back to match the high-z sample, would not be recognized as being passive objects (van Dokkum & Franx 2001; Saglia et al. 2010; Valentinuzzi et al. 2010a,b). For the SPIDER sample, luminosity-weighted ages are available (Swindle et al. 2011). These ages are derived from the spectral fitting code STARLIGHT (Cid Fernandes et al. 2005), which finds the best combination of simple

stellar populations (SSPs) (with free age, metallicity and alpha enhancement) which reproduce the measured spectra. Thus, we only take those SPIDER objects which have an age ≥ 1.5 Gyr, at the average redshift of the EDisCS sample (i.e. older than 7.5 Gyr). In contrast, for the T+09 data sample, ages estimated fitting exponential star formations (SFs) (with characteristic time-scale τ) to optical colours are available (T+09; Napolitano et al. 2010). For these reasons, we have only taken those systems that after a time τ (corresponding to the epoch when the SF is reduced to 37 per cent of the initial value) are older than the look-back time at the average redshift of the sample. The results are fairly unchanged if we use the epoch when the SF is ~ 14 per cent of the initial value (i.e. at the epoch 2τ). Ages for ATLAS[3D] are not available; for this reason the impact of progenitor bias will not be discussed for this data set.

The outcomes for such old systems are shown in Fig. 2 as red and green lines for SPIDER and T+09 data samples, respectively. The impact on the results is very weak (e.g. Belli, Newman & Ellis 2014), and it is possibly more relevant in the $\sigma_{\rm e}$–$M_\star$ correlation. We notice that in the two data samples, the impact of the progenitor bias pushes the $R_{\rm e}$ in the two opposite directions, since the correlation between $R_{\rm e}$ and galaxy age is still controversial. In fact, contrasting results are found by observational analysis, which find that at fixed mass/σ, younger systems are larger (Shankar & Bernardi 2009; Napolitano et al. 2010; Valentinuzzi et al. 2010a) or are as sized as older galaxies (Graves, Faber & Schiavon 2009). The outcomes from semi-analytic galaxy formation models are also still unclear, as there are results showing that younger galaxies are larger (Khochfar & Silk 2006) or also smaller (Shankar et al. 2010) than the oldest systems.

Despite these uncertainties, in the following we will discuss the results with and without the progenitor bias for those samples for which this has been computed (i.e. SPIDER and T+09).

4 DM EVOLUTION

In this section, we investigate the galaxy central DM content as a function of z. To quantify that, we will use either the de-projected DM fraction at $R_{\rm e}$, $f_{\rm DM} = 1 - M_\star(R_{\rm e})/M_{\rm tot}(R_{\rm e})$, or the de-projected total-to-stellar mass ratio at $R_{\rm e}$, $M_{\rm tot}(R_{\rm e})/M_\star(R_{\rm e})$. The latter will be useful to avoid unphysical negative $f_{\rm DM}$ values, in particular when computing the best-fitting relations among galaxy parameters.

From the previous section, we have seen that there is almost no evolution in the relation $\sigma_{\rm e}$–$M_\star$, and this might suggest that so would be for the $M_{\rm tot}(r)/M_\star(r)$, if the $\sigma_{\rm e}$ is a fair proxy of the total mass. On the other hand, we have observed a strong evolution of the $R_{\rm e}$ with the stellar mass, which shows that the scale where most

---

[1] The shallower size–mass relations found in T+09 and ATLAS[3D] with respect to the SPIDER sample are explained by the fact that fitting a high-n galaxy with a de Vaucouleurs profile gives a systematically smaller $R_{\rm e}$ value, hence flattening the size–mass relation.
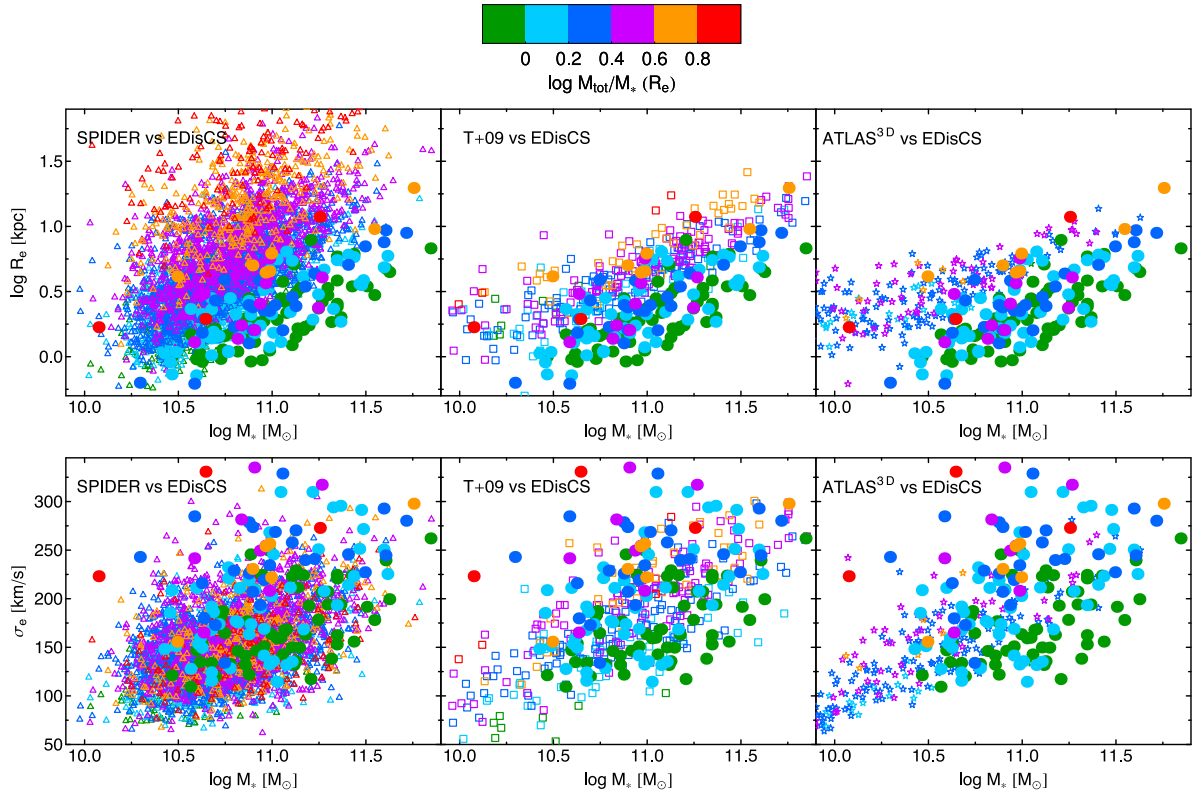
Figure 3. Size–mass (top panels) and σ_e–mass (bottom panels) relations colourized according to the $M_{tot}/M_\star$ bins in the colour bar (grayscale bar in the B&W version) in the top. We show single data points as in Fig. 1.

of the mass in stars is confined was more compact in the earlier epochs with respect to present time (even in case the progenitor bias is taken into account). Thus, in the second part of the present section, we will discuss the role of this size evolution in our DM inferences.

4.1 DM content and correlations

In Fig. 3, we start by re-proposing the R_e–$M_\star$ and σ_e–$M_\star$ correlations (see Fig. 1), now colourized according to the $M_{tot}/M_\star$. The average $M_{tot}/M_\star$ are also plotted as a function of R_e, $M_\star$ and σ_e in Fig. 4 and the best-fitting relations listed in Table 2.

4.1.1 Results

As for the R_e–$M_\star$ and σ_e–$M_\star$ correlations, in local galaxies the DM trends are nearly independent of the sample adopted. In agreement with the local samples, the high-z galaxies from EDisCS preserve almost all the DM trends against stellar mass, central velocity dispersion and effective radius (see Figs 3 and 4), with almost all correlations being significant at more than 99 per cent. However, a clear offset in the correlations is evident. In Fig. 3, we find that at fixed $M_\star$, EDisCS galaxies present similar σ_e, but smaller R_e and $M_{tot}/M_\star$ with respect to local galaxy samples. This is made even clearer in Fig. 4, where the $M_{tot}/M_\star$ median relations are shown. Here, the EDisCS galaxies are more DM dominated at larger R_e and σ_e (i.e. they follow a positive correlation) along a trend which runs almost parallel to the local sample but shifted towards lower $M_{tot}/M_\star$ (see Table 2). In particular, we note that at any fixed R_e, the EDisCS sample presents $M_{tot}/M_\star$ of ∼0.15–0.25 dex smaller than the ones at low z. These differences are all significant at more than

3σ, as evident from the linear regressions in Table 2. If R_e was the only responsible for the $M_{tot}/M_\star$–z variation, one would expect statistically no variation of the $M_{tot}/M_\star$–R_e with z.

In the same figure, we also observe that the change in $M_{tot}/M_\star$ is stronger at any fixed $M_\star$ and σ_e, being the average offset between the high- and low-redshift samples of $M_{tot}/M_\star$ ∼0.3–0.35 and ∼0.5–0.6 dex, respectively, for the two quantities. Particularly interesting is the $M_{tot}/M_\star$–$M_\star$ correlation which changes the slope from the low- to the high-z trend, although consistent within the errors with null value (see Table 2). The latter, together with the presence of a marginal evolution also of the $M_{tot}/M_\star$–R_e in the top panel, show that the $M_{tot}/M_\star$ evolution with z cannot be driven by the R_e only, although previous analyses have shown that the main driver of most of the scaling relations involving the central DM fraction in ETGs is the effective radius (e.g. Auger et al. 2010; Napolitano et al. 2010; Tortora et al. 2010b, 2012), and there are accumulating pieces of evidence that R_e scales with the redshift (Trujillo et al. 2006, 2011; Saglia et al. 2010, see also the top panels of Fig. 2). Despite the fact that the R_e–z relation might be a key factor for interpreting the $M_{tot}/M_\star$–z trend, there have to be mechanisms related to the global stellar and dark mass assembly which also shape the $M_{tot}/M_\star$ trend with z. We will discuss the possible evolution scenarios later in Section 4.2; here we note that, taking the current $M_{tot}/M_\star$ results at face values, the evolution of this quantity is evident from Figs 3 and 4, which has increased with time across the last ∼7 Gyr. Indeed, this observed evolution in $M_{tot}/M_\star$ is also found if we split the EDisCS sample into two redshift bins (see Fig. 4 and Table 2).

In Fig. 5, we summarize the average results for the Chabrier IMF and the bottom-heavier Salpeter IMF, this time represented as the DM fraction, f_{DM}, as a function of redshift (on the right axes the corresponding $M_{tot}/M_\star$ are also shown). The increasing
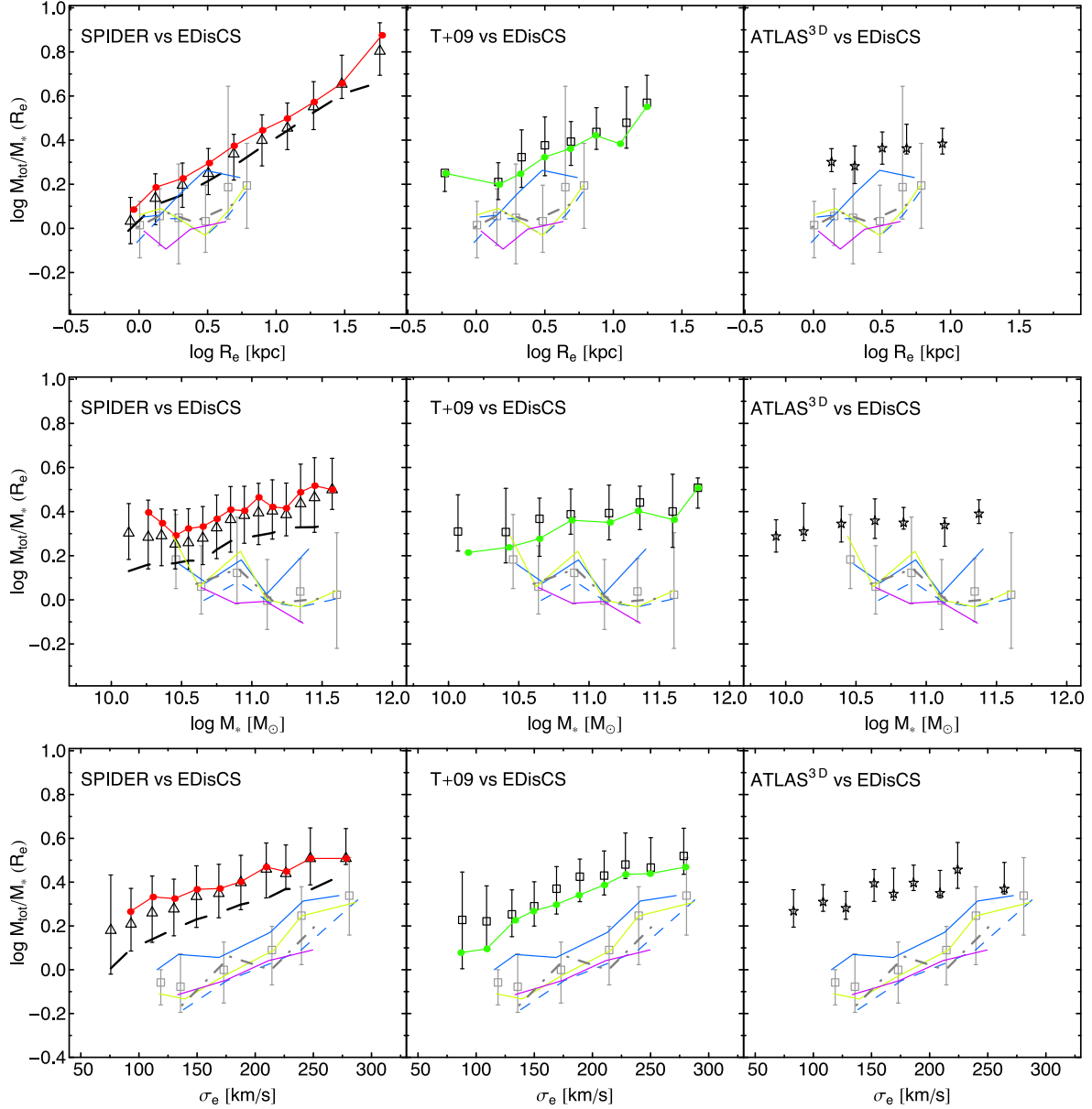
Figure 4. $M_{tot}/M_\star$ (in logarithmic scale) as a function of R_e (top panels), $M_\star$ (middle panels) and σ_e (bottom panels). Symbols are as in Fig. 2. The dashed line is made calculating the SPIDER K-band profiles at $R_{e,K}$. The yellow lines (black in the B&W version) are for the roundest EDisCS objects with axial ratio, $q > 0.6$. Purple lines (short dashed black in the B&W version) are for field EDisCS systems. Grey point–dashed lines are for EDisCS elliptical morphologically selected (i.e. with $T \geq -4$).

Table 2. Best-fitting parameters for the relation $M_{tot}/M_\star - R_e$, $M_{tot}/M_\star - M_\star$ and $M_{tot}/M_\star - \sigma_e$. The following best relations are fitted: $\log M_{tot}/M_\star = a + b \log (R_e/2\,\mathrm{kpc})$, $\log M_{tot}/M_\star = a + b \log (M_\star/10^{11}\,\mathrm{M_\odot})$ and $\log M_{tot}/M_\star = a + b \log (\sigma_e/200\,\mathrm{km\,s^{-1}})$. Best value, 1σ error and significance of the correlation are shown.

Sample	$M_{tot}/M_\star - R_e$			$M_{tot}/M_\star - M_\star$			$M_{tot}/M_\star - \sigma_e$		
	a	b	Significance	a	b	Significance	a	b	Significance
SPIDER	0.18 ± 0.01	0.40 ± 0.02	99 per cent	0.38 ± 0.01	0.17 ± 0.03	99 per cent	0.05 ± 0.03	0.36 ± 0.03	99 per cent
T+09	0.29 ± 0.02	0.28 ± 0.04	99 per cent	0.40 ± 0.02	0.06 ± 0.04	99 per cent	0.05 ± 0.06	0.36 ± 0.06	99 per cent
ATLAS^{3D}	0.31 ± 0.02	0.16 ± 0.05	99 per cent	0.36 ± 0.01	0.04 ± 0.02	99 per cent	0.21 ± 0.05	0.17 ± 0.06	99 per cent
EDisCS	0.07 ± 0.03	0.20 ± 0.10	99 per cent	0.08 ± 0.03	-0.17 ± 0.12	95 per cent	-0.42 ± 0.13	0.52 ± 0.12	99 per cent
EDisCS – low z	0.14 ± 0.05	0.26 ± 0.13	99 per cent	0.16 ± 0.05	0.05 ± 0.16	95 per cent	-0.27 ± 0.10	0.46 ± 0.11	99 per cent
EDisCS – high z	0.01 ± 0.05	0.23 ± 0.15	99 per cent	0.03 ± 0.05	-0.08 ± 0.20	95 per cent	-0.59 ± 0.12	0.61 ± 0.12	99 per cent

The net conclusion of this analysis is that according to the $f_{\rm DM}$ variation with z, the IMF which would be compatible with physical $f_{\rm DM}$ values can range from bottom-heavy to bottom-light at low z, but it does not have the same leverage at higher z (e.g. $z \gtrsim 0.6$), where the IMF has to be mainly bottom-light (e.g. Chabrier-like), and compatible with a Salpeter IMF in very high $\sigma_{\rm e}$ systems only, producing negative DM fractions just in a few of systems.

A detailed investigation of the IMF variation with $\sigma_{\rm e}$ as a function of z is beyond the scope of this paper. Therefore, in the following we will discuss the results based on a constant IMF across the look-back time.

4.1.2 Systematics

We have seen that the IMF is a major source of uncertainty in the $f_{\rm DM}$ trend with z. However, there are other sources of systematics that may provide alternative explanations for the negative $f_{\rm DM}$ values of the EDisCS sample within 1 $R_{\rm e}$ and eventually modify our trends with redshift. Besides systematics in the stellar mass estimates, the negative $f_{\rm DM}$ values can be due to measurement errors on galaxy parameters and/or a failure of the mass model adopted for the $M_{\rm dyn}$ (e.g. Tortora et al. 2012). A brief discussion of all possible systematics is given here below.

(i) We measure $R_{\rm e}$s using I-band photometry, which means that $R_{\rm e}$s are approximately the rest-frame V and B bands, respectively, at $z \sim 0.4$ and $z \sim 0.8$. $R_{\rm e}$s are found to be larger at smaller wavelengths (Sparks & Jorgensen 1993; La Barbera & de Carvalho 2009; Roche, Bernardi & Hyde 2010; Vulcani et al. 2014). In particular, using a sample of galaxies with $z < 0.3$, Vulcani et al. (2014) estimate an increase from g to u and from r to g band of $\lesssim$ 15 per cent, and similar results are found in La Barbera & de Carvalho (2009) following the method in Sparks & Jorgensen (1993). For this reason, our $R_{\rm e}$s which are measured in the rest-frame V band at the smallest EDisCS redshifts are conservative lower limits and would be larger if calculated in the same rest frame as the highest redshift ETGs. Thus, stronger evolution of $R_{\rm e}$ and $f_{\rm DM}$ with redshift is expected if this effect would be taken properly into account. We have shown the impact of waveband in Fig. 4 for the SPIDER $M_{\rm tot}/M_{\star}$ where the profiles are calculated at K-band $R_{\rm e}$, which are smaller than our reference values. This reduces the difference with EDisCS galaxies with respect to the results from g-band light profile and g-band $R_{\rm e}$ (not shown in the figure for brevity) which would give $M_{\rm tot}/M_{\star}$ larger than our reference estimates.

(ii) In addition to uncertainties in stellar mass estimates, the choice of the mass profile that we have made (i.e. the SIS model) can be inappropriate for low-$\sigma_{\rm e}$ (or $M_{\star}$) galaxies and cause an excess of negative $M_{\rm tot}/M_{\star}$ values, mainly at high z (e.g. Sonnenfeld et al. 2013). In particular, $M_{\rm tot}/M_{\star}$ and the slope of total mass density are tightly correlated, with shallower density profiles corresponding to larger $M_{\rm tot}/M_{\star}$ (Humphrey & Buote 2010; Remus et al. 2013; Dutton & Treu 2014). To quantify the impact of a free total mass density slope, α, we have adopted a power-law mass density $\rho \propto r^{\alpha}$, with slope steeper and shallower than isothermal. We use the two extreme values $\alpha = -2.5$ and -1.5, which bracket most of the results in the literature. We find that the average $M_{\rm tot}/M_{\star}$ gets smaller (larger) of 0.12 (0.05) dex for $\alpha = -2.5$ ($=-1.5$); in a realistic case with a varying slope with mass, smaller changes, < 0.12 dex, will be found (e.g. Dutton & Treu 2014). If α is constant with time, then these corrections have to be applied to both local and EDisCS samples, and our results are left naturally unaffected. On the other hand, if we assume for local ETGs that the slope is varying with mass

Figure 5. Average DM fraction evolution. Symbols for local samples, assuming a Chabrier IMF, are as in Figs 2 and 4. Red and blue symbols are for lower z and higher z EDisCS galaxies. Solid line connects these data points. Dashed line connects the results for a Salpeter IMF. The grey region sets the locus of unphysical (i.e. negative) DM fractions. Solid green line is for a toy model assuming a Chabrier (Salpeter) IMF at high (low) redshift. Solid orange line is for a toy model assuming the local $\delta_{\rm IMF}$–$\sigma_{\rm e}$ relation from Tortora et al. (2013).

trend of the $f_{\rm DM}$ at lower z is now explicitly evident, which is the consequence of the offset of the $M_{\rm tot}/M_{\star}$ between the low- and high-z samples, as discussed before. In the same figure, we plot the regions of 'unphysical' $f_{\rm DM}$ as a shadowed area. Here, the lower $M_{\rm tot}/M_{\star}$ of the high-z sample (green points in Fig. 3) implies a much higher fraction of (unphysical) negative $f_{\rm DM}$ (57 out 154 galaxies, i.e. 37 per cent) assuming a Chabrier IMF, which becomes even more dramatic if a Salpeter IMF is assumed (115 out of 154, i.e. 75 per cent). A fraction of these galaxies with negative $f_{\rm DM}$ would be compatible with observational scatter in $M_{\star}$ and $M_{\rm tot}$ (e.g. appendix A in Napolitano et al. 2010). However, it is difficult to explain all the negative $f_{\rm DM}$ as a consequence of this observational scatter, rather this may suggest that the bottom-heavy Salpeter IMF is disfavoured with respect to a Chabrier IMF.

Hence, the inferred $f_{\rm DM}$ from a Salpeter IMF (or bottom-heavier IMFs in general) are disfavoured with respect to a Chabrier IMF, mainly at high redshift ($z \gtrsim 0.6$). In order to reduce this tension, one can relax the assumption of IMF universality, and re-compute the effect on the median $f_{\rm DM}$s as a function of z by assuming Salpeter and Chabrier IMFs in local and EDisCS samples, respectively: this very crude assumption would cancel out the variation of $f_{\rm DM}$ with redshift as shown by the green line in Fig. 5.

A more reasonable assumption for a non-universal IMF should take into account also some variation in terms of mass, as found in local analysis (Cappellari et al. 2012; Conroy & van Dokkum 2012; Spiniello et al. 2012; Dutton et al. 2013; Ferreras et al. 2013; Goudfrooij & Kruijssen 2013; La Barbera et al. 2013; Tortora et al. 2013, 2014; Weidner et al. 2013). We have also evaluated this effect by correcting the DM fractions for all the samples using the same local relation between $\delta_{\rm IMF} = \Upsilon_{\star}/\Upsilon_{\star,\rm Chabrier}$ and $\sigma_{\rm e}$ from Tortora et al. (2013). In this case, some $f_{\rm DM}$ trend with redshift is still observed (see the orange line in Fig. 5), but the number of high-z galaxies with negative DM (mainly with small $\sigma_{\rm e}$) is still too large to accommodate these systems without a variation of IMF across the cosmic time.

as it is effectively found, then the only way to totally remove any $M_{tot}/M_\star$ evolution is that EDisCS galaxies have total mass density slopes very shallow ($\alpha > -1.5$, and consequently larger $M_{tot}/M_\star$), which is not expected, since at high redshifts, where gas and *in situ* star formation dominate the galaxies, the ETGs from cosmological simulations have a total density slope very steep ($\alpha \sim -3$), and mergings tend to drive the galaxy to a nearly isothermal profile (Remus et al. 2013). Thus, although a varying slope with redshift has to be further investigated, our tests showed that the conclusions of the present paper are left nearly unchanged.

(iii) If rotation velocities would be included in the analysis, M_{dyn} would get higher, reducing the fraction of negative f_{DM}s.

(iv) As discussed in Section 3, galaxies which are star forming at the cosmic epoch of the EDisCS galaxies have to be removed. Thus, progenitor bias has to be applied, and we plot the results in Fig. 4. As for the trends of R_e and σ_e as a function of $M_\star$, the $M_{tot}/M_\star$ results are only little affected. In particular, the inclusion of the progenitor bias makes the $M_{tot}/M_\star$ larger (smaller) for SPIDER (T+09) samples. See Napolitano et al. (2010) for further details about the f_{DM}–age correlation (see also Tortora et al. 2010b). We notice that after the progenitor bias is applied, the median $M_{tot}/M_\star$ only slightly changes, since the largest fraction of galaxies (the oldest) is left unchanged.

(v) We have checked the effect of the ellipticity on the mass inferences and restricted the analysis to EDisCS objects with axial ratio $q > 0.6$ (60 per cent of the full sample, see yellow lines in Fig. 4), in order to limit to the roundest galaxies. The overall results are practically unchanged.

(vi) The results are also almost unchanged if we only take those objects with morphological type of pure ellipticals (i.e. $T \leq -4$). Both tests on the ellipticity (point (v)) and morphology above give support to the negligible impact of ordered motion on our M_{dyn} estimates.

(vii) Finally, we find that $M_{tot}/M_\star$ in field galaxies are slightly smaller than those in cluster galaxies (consistently with the stronger evolution found in the literature; Saglia et al. 2010), but due to the scatter in the sample and uncertainties this difference is not statistically relevant, pointing to a central DM content which is almost independent of the environment the galaxy lives in (accordingly to a similar analysis in local environments; Tortora et al. 2012).

4.2 Passive evolution versus accretion by merging

We complement the analysis performed in the previous section by discussing our results within the two dominant evolution scenarios: i.e. passive evolution from monolithic collapse and galaxy mergers from the hierarchical model.

4.2.1 Passive evolution

We start from discussing a pseudo-passive evolution, assuming no merging, and compute the ageing of stellar populations in our sample. The EDisCS galaxies, as spectroscopically selected passive objects, have low residual SF and can be fairly approximated by a single burst SSP, or at most a short-duration SF. We consider SPS models from Bruzual & Charlot (2003) and adopt an exponential SF with time-scale of $\tau = 500$ Myr (T+09) and different formation redshifts ($z_f = 1.5, 2.5, 3$). On average, for passive evolution the EDisCS stellar mass becomes smaller by 0.01–0.02 dex, due to mass-loss. This very mild evolution is not enough to produce the local R_e–$M_\star$ relations and similarly the local DM correlations. Longer

SF history with $\tau > 1$ Gyr would increase the $M_\star$, increasing the discrepancies with the local observed local samples.

4.2.2 Hierarchical scenario

Alternatively, galaxy mergers seem to be the natural mechanisms that can account for both size and mass accretion. Simulations of dissipationless major mergers of elliptical galaxies in Boylan-Kolchin, Ma & Quataert (2005) have predicted the change in central DM in the merger remnant. They demonstrate that the DM fraction within a certain physical radius decreases a bit after the merger. But the DM fraction within the final R_e is greater than the DM fraction within the initial R_e, because $M_{tot}(R_e)$ changes after the merger more than $M_\star(R_e)$ (see also below for more quantitative details).

The effect of merging on the central f_{DM} has been investigated in detail with *N*-body simulations by Hilz et al. (2013). Here, three fiducial models with mass ratio of 1:1, 5:1 and 10:1 are analysed to find that, at different final stellar masses, the equal-mass mergers produce a smaller size increase of multiple minor mergers. In particular, the variation of R_e with respect to the initial radius, R_e/R_0, in terms of the variation of $M_\star$ with respect to the initial stellar mass, $M_\star/M_0$, is found to be $R_e/R_0 \propto (M_\star/M_0)^{0.91}$ for the equal-mass merger and $\propto (M_\star/M_0)^{2.4}$ for the minor mergers. The latter predictions on the R_e and $M_\star$ accretion have been found to be consistent with observations (van Dokkum et al. 2010).

Taking these results into account, we have constructed some toy models assuming that $M_{DM} \propto M_{vir} r^\eta$ around R_e, with $\eta \sim 2$ for a standard NFW and $\eta \sim 1.2$ for a contracted NFW, hereafter AC+NFW (according with Boylan-Kolchin et al. 2005). Consistently with Hilz et al. (2013), we have also taken the average evolution of R_e in terms of $M_\star$ evolution for the equal-mass merging (i.e. $R_e/R_0 \propto (M_\star/M_0)^{0.91}$) and minor merging (i.e. $R_e/R_0 \propto (M_\star/M_0)^{2.4}$) with the further assumption that the variation of the virial mass almost follows the one of the stellar mass, i.e. $\delta M_{vir} \approx \delta M_\star$. This intrinsically reflects the hypothesis that the systems concurring to mergings all have some constant $M_{vir}/M_\star$, which is reasonable for most of the stellar mass range covered by our sample.

These simplified models have the advantage of dealing with a limited number of parameters, but still providing a quantitative assessment of the impact of the evolution scenario on the observed DM fractions. In particular, we need to clarify whether the observed DM fraction evolution is compatible with a variation with z of R_e and $M_{tot}/M_\star$, or rather it is the IMF variation with z, the only viable explanation of the observed correlations.

In Fig. 6, we show the predicted evolved tracks for the median R_e and $M_{tot}/M_\star$ of the EDisCS data set corresponding to a median $\log M_\star/M_\odot = 11$. We have considered the evolution tracks related to different merging types, according to the list in Table 3. The major merging tracks are shown as blue lines with dots/squares indicating the events corresponding to $x \times M_0$ ($x = 0, 1, 2, \ldots, n$) mass increments, while the minor merging tracks are shown by yellow lines where dots/squares indicate the $x \times M_0$ with $x = 0, 0.5, 1, \ldots, n$. Dots and squares are for NFW and AC+NFW profiles, respectively.

Comparing the model predictions with local results, we see that after a single major merger, it is not possible to reproduce the local correlations (blue lines in R_e–$M_\star$ and $M_{tot}/M_\star$–$M_\star$). Adopting an NFW profile (Major NFW), after ~ 3 major mergers the high-z galaxy moves along the track to overlap the local observed $M_{tot}/M_\star$, while it would need more merging events if a AC+NFW is used
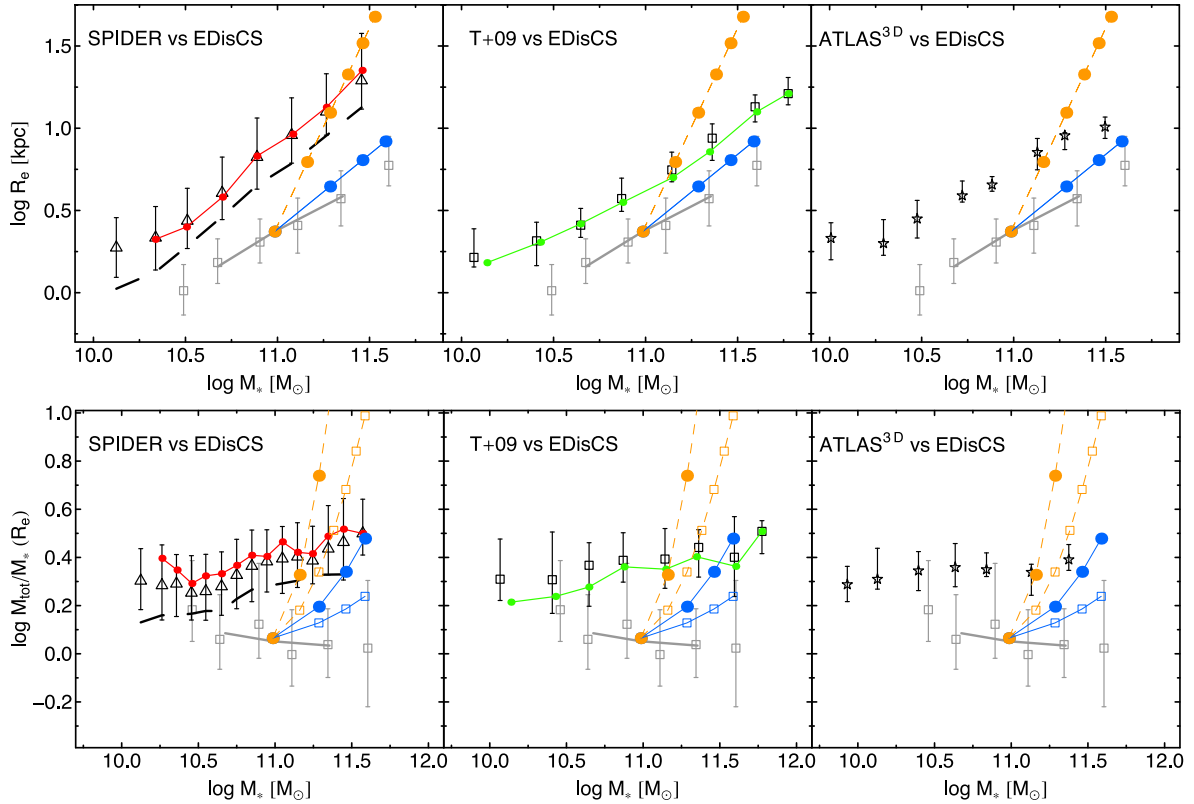
Figure 6. Evolution of R_e–$M_\star$ (top panels) and $M_{tot}/M_\star$–$M_\star$ (bottom panels). The symbols for local and EDisCS samples are the same as in Figs 2 and 4. The grey line is for EDisCS sample, but averaging over only three mass bins. We take as example the average galaxy at log $M_\star/M_\odot = 11$ and evolve it accordingly to the toy models discussed in the text and in Table 3. Blue and orange tracks are for major and minor mergings, respectively. Dots and squares are for the NFW and AC+NFW profiles, and set the R_e, $M_\star$ and $M_{tot}/M_\star$ after each single merging. Of course, the DM model only impacts the $M_{tot}/M_\star$–$M_\star$ trends. Notice that for the minor merging case, dots and squares mark the epochs when one-half of the initial mass is accreted.

Table 3. Typical parameters of toy models for major and minor mergings. See the text for details. The predictions for R_e and $M_{tot}/M_\star$ are plotted in Fig. 6: Major NFW (blue lines and dots), Minor NFW (yellow lines and dots), Major AC+NFW (blue lines and squares) and Minor AC+NFW (yellow lines and squares). See the text and caption of Fig. 6 for further details.

Model	$M_\star/M_0$	Merging type	η
Major NFW	1,2,3	Major	2
Minor NFW	0.5,1,1.5,...	Minor	2
Major AC+NFW	1,2,3	Major	1.2
Minor AC+NFW	0.5,1,1.5,...	Minor	1.2

(Major AC+NFW, open squares). In both cases, though, the toy-model predictions do not match the average local R_e–$M_\star$ relations, showing a deficiency of size growth expected for major merging events.

In contrast, after a few minor mergers (yellow lines) which accrete ∼0.5–1.5 of the initial $M_\star$ (depending on the DM profile adopted), both R_e–$M_\star$ and $M_{tot}/M_\star$–$M_\star$ are matched (see Minor NFW and Minor AC+NFW).

To summarize the behaviour of our toy models: (a) the impact of minor merging on R_e and $M_{tot}/M_\star$ is stronger than the one of major merging at fixed accreted $M_\star$, and the latter do not seem to account for the observed R_e evolution; (b) uncontracted NFW models provide larger $M_{tot}/M_\star$.

For simplicity, we have not analysed here the case of M_{vir} which changes less (more) than $M_\star$, i.e. $\delta M_{vir} < \delta M_\star$ ($\delta M_{vir} > \delta M_\star$). For example, if $\delta M_{vir} > \delta M_\star$, then M_{dyn} and $M_{tot}/M_\star$ get larger.

In Section 4.1, we have shown that $M_{tot}/M_\star$ are slightly smaller in field than in cluster galaxies, but this difference is not statistically significant. For galaxies living within dense environments, the chance to interact with neighbouring galaxies is very high, but for galaxies in the field merging is a less common event. Thus, the only ways to put EDisCS field galaxies and local objects within a coherent scenario are (a) they will fall in the following 7 Gyr within a cluster or a group of galaxies, and merge with other galaxies, (b) they are atypical objects which set out of the median local relations, (c) any other phenomenon is working to puffing up the galaxy size (as AGN feedback; Fan et al. 2008, 2010) and consequently the $M_{tot}/M_\star$.

5 CONCLUSIONS

We have analysed the central DM content in a sample of high-z (∼0.4–0.8) ETGs from the EDisCS survey, parametrized in this paper through the total-to-stellar mass ratio, $M_{tot}/M_\star$, (calculated at $r = 1 R_e$), and compared the results with local galaxy samples (SPIDER, Tortora et al. 2012; ATLAS3D, T+09; Cappellari et al. 2011).

We have shown that local correlations between $M_{tot}/M_\star$ and R_e, and $M_\star$ and σ_e, are fairly independent of the sample adopted and almost all conserved at high z (see Fig. 4). In fact, high-z galaxies are more DM dominated at larger R_e and σ_e (i.e. they follow a

positive correlation). For this sample, this is a clear indication that the main driver in the observed positive correlations is the effective radius, consistently with local galaxies as found in Napolitano et al. (2010, see also Auger et al. 2010; Tortora et al. 2010b, 2012). A less significant negative correlation is found in terms of stellar mass, in the opposite direction to the correlations of the local galaxies.

As seen in Figs 3 and 4, an overall offset of the $M_{tot}/M_\star$ from high- to low-z galaxies is evident, suggesting an evolution of the DM fraction within R_e. In particular, we find that at fixed R_e, the EDisCS sample presents $M_{tot}/M_\star$ of $\sim$0.15–0.25 dex smaller than local galaxies. The change in $M_{tot}/M_\star$ is stronger at $M_\star$ and σ_e fixed, being $\sim$0.3–0.35 and $\sim$0.5–0.6 dex, respectively. At fixed $M_\star$, a clear variation of the $M_{tot}/M_\star$ as a function of R_e is found from high- to low-z galaxies (Fig. 3), but not in σ_e (Fig. 1). The overall evolution of the DM fraction with redshift (see Fig. 5) is consistent with the results found in Faure et al. (2011), but in contrast with the opposite trend found by Ruff et al. (2011, within $R_e/2$), which find larger DM fractions at high z, and inconsistent with the absence of evolution in Bezanson et al. (2013). Our findings are consistent with results in Beifiori et al. (2014) which, using SDSS-III/BOSS and SDSS-II data sets, find smaller DM fractions in higher z galaxies, but the trend with redshift is shallower than ours. Instead, we do not agree with the absence of evolution found in Belli et al. (2014) for a sample of quiescent galaxies at $z > 1$.

We find that, on average, the inferred f_{DM} from a Salpeter IMF (or bottom-heavier IMFs in general) are disfavoured with respect to a Chabrier IMF, mainly at high redshift and in low-σ_e systems. Thus, we can reproduce our f_{DM} assuming a Chabrier/Salpeter IMF at high/low redshift, which would point to an IMF evolution with redshift. This result seems to be in contrast with the recent findings in Shetty & Cappellari (2014), who find a Salpeter IMF in $z \sim 0.7$–0.8 massive galaxies. However, their models assume a constant-M/L profile, and no DM content in the central regions (i.e. the mass is only in stars) which might have biased the overall stellar M/L as their dynamical M/L and the inferred $\Upsilon_\star$ are just upper limits (Tortora et al. 2013). Furthermore, their sample is composed of very massive ($M_\star \gtrsim 10^{11} M_\odot$) galaxies with very high σ (most of the systems have $\sigma > 200$ km s^{-1}). Taking all these specifics of their sample, their results are substantially consistent with ours, since a Salpeter IMF is allowed by the EDisCS systems at similar velocity dispersions, providing nearly null DM fractions consistent with their assumption (see bottom panels in Fig. 4).

We have briefly discussed the possibility that the IMF is non-universal, not only as a function of redshift, but that it can also vary with the mass/central velocity dispersion (see e.g. Tortora et al. 2013). The impact on our results of a more realistic IMF variation with σ_e from local observations (Tortora et al. 2013) has been analysed, and assumed to be valid and the same at all redshifts. This has been shown to produce a smaller number of negative DM fractions with respect to a Salpeter IMF. However, a combined evolution with mass/σ_e and redshift would completely solve the issue of negative f_{DM}. Although most of stars are already in place at $z < 1$, a change of IMF across the time could be produced by two different processes: (a) new stars formed in the core during a wet merging process, which also produce positive age gradients (e.g. Hopkins et al. 2008; Tortora et al. 2010a) and 'higher mass' IMF (Napolitano 2010) in young and massive local ETGs, or (b) by stars from both merging galaxies characterized by two different IMFs, which can combine to modify the cumulative IMF of the remnant. Unfortunately, the net effect of these processes on the final IMF is not yet clear, and in most cases the combination of a 'higher' and a 'lower mass' IMF would produce a final diluted IMF.

Therefore, it is also plausible to scan alternative mass modelling and mechanisms to explain the negative f_{DM} at high z and in low-σ_e ETGs, as (i) adopting realistic and viable DM halo profiles, (ii) the effect of some dissipative processes that might alter the standard DM distribution like the adiabatic contraction (Napolitano et al. 2010; Tortora et al. 2013) or (iii) some other DM flavour (e.g. some warm DM; Schneider et al. 2012).

However, a detailed analysis of the IMF and DM halo evolution across the time is beyond the scopes of this paper and will be addressed in future, assuming more complex mass modelling (Tortora et al. 2013, 2014). From the theoretic point of view, this evolution would pose a further open question: Which circumstances might have caused the IMF variation across time at any given $M_\star$? This is a new fundamental question which has to be added to the IMF evidence of non-universality (Cappellari et al. 2012; Conroy & van Dokkum 2012; Spiniello et al. 2012; Dutton et al. 2013; Ferreras et al. 2013; Goudfrooij & Kruijssen 2013; La Barbera et al. 2013; Tortora et al. 2013, 2014; Weidner et al. 2013).

We have finally investigated our results with a fixed IMF within galaxy formation scenarios and found that simple passive evolution is not able to reproduce local results. In contrast, the galaxy merging scenario allows us to reproduce the growth of the R_e and the $M_{tot}/M_\star$ with z. We have used toy models which take into account size and mass accretion from minor and major mergings to show that a single major merger is not able to reproduce local correlations, while many minor mergers work better (e.g. Hilz et al. 2013; Belli et al. 2014).

Of course, in order to have a firmer assessment on the actual DM content evolution with redshift, much larger samples are needed, with full spectroscopic and photometric information. In particular, gravitational lensing can provide us very robust mass estimates (e.g. Barnabè et al. 2009, 2011; Covone et al. 2009; Auger et al. 2010; Tortora et al. 2010b; Spiniello et al. 2011). Thus, survey projects like SLACS or COSMOS (e.g. Faure et al. 2008) or the ongoing European Southern Observatory public surveys with VST telescope (such as KiDS) together with spectroscopic surveys (e.g. BOSS/SDSS, Thomas et al. 2013; Beifiori et al. 2014 and GAMA, Baldry et al. 2010) are fundamental to collect a large sample of galaxies, which span a wide range of luminosity and redshifts, in order to probe more massive galaxies in the universe and their evolutive history, by means of the description of the different history of stellar and DM and their interplay in the inner and outer regions of galaxies.

ACKNOWLEDGEMENTS

REFERENCES

Abazajian K. et al., 2003, AJ, 126, 2081
Abazajian K. N. et al., 2009, ApJS, 182, 543
Adelman-McCarthy J. K. et al., 2008, ApJS, 175, 297
Auger M. W., Treu T., Bolton A. S., Gavazzi R., Koopmans L. V. E., Marshall
    P. J., Bundy K., Moustakas L. A., 2009, ApJ, 705, 1099
Auger M. W., Treu T., Bolton A. S., Gavazzi R., Koopmans L. V. E., Marshall
    P. J., Moustakas L. A., Burles S., 2010, ApJ, 724, 511
Baldry I. K. et al., 2010, MNRAS, 404, 86
Barnabè M., Czoske O., Koopmans L. V. E., Treu T., Bolton A. S., Gavazzi
    R., 2009, MNRAS, 399, 21

Barnabè M., Czoske O., Koopmans L. V. E., Treu T., Bolton A. S., 2011, MNRAS, 415, 2215

Beifiori A. et al., 2014, ApJ, 789, 92

Bell E. F., de Jong R. S., 2001, ApJ, 550, 212

Belli S., Newman A. B., Ellis R. S., 2014, ApJ, 783, 117

Benson A. J., Cole S., Frenk C. S., Baugh C. M., Lacey C. G., 2000, MNRAS, 311, 793

Bezanson R., van Dokkum P. G., van de Sande J., Franx M., Leja J., Kriek M., 2013, ApJ, 779, L21

Bolton A. S., Burles S., Koopmans L. V. E., Treu T., Moustakas L. A., 2006, ApJ, 638, 703

Bolton A. S., Burles S., Koopmans L. V. E., Treu T., Gavazzi R., Moustakas L. A., Wayth R., Schlegel D. J., 2008, ApJ, 682, 964

Boylan-Kolchin M., Ma C.-P., Quataert E., 2005, MNRAS, 362, 184

Bruzual G., Charlot S., 2003, MNRAS, 344, 1000

Bullock J. S., Kolatt T. S., Sigad Y., Somerville R. S., Kravtsov A. V., Klypin A. A., Primack J. R., Dekel A., 2001, MNRAS, 321, 559

Cappellari M. et al., 2006, MNRAS, 366, 1126

Cappellari M. et al., 2011, MNRAS, 413, 813

Cappellari M. et al., 2012, Nature, 484, 485

Cappellari M. et al., 2013a, MNRAS, 432, 1709

Cappellari M. et al., 2013b, MNRAS, 432, 1862

Cardone V. F., Tortora C., 2010, MNRAS, 409, 1570

Cardone V. F., Tortora C., Molinaro R., Salzano V., 2009, A&A, 504, 769

Cardone V. F., Del Popolo A., Tortora C., Napolitano N. R., 2011, MNRAS, 416, 1822

Cenarro A. J., Trujillo I., 2009, ApJ, 696, L43

Chabrier G., 2001, ApJ, 554, 1274

Chae K.-H., Bernardi M., Kravtsov A. V., 2014, MNRAS, 437, 3670

Cid Fernandes R., Mateus A., Sodré L., Stasińska G., Gomes J. M., 2005, MNRAS, 358, 363

Conroy C., van Dokkum P. G., 2012, ApJ, 760, 71

Conroy C., Wechsler R. H., 2009, ApJ, 696, 620

Covone G. et al., 2009, ApJ, 691, 531

de Vaucouleurs G., 1948, Ann. Astrophys., 11, 247

Dutton A. A., Treu T., 2014, MNRAS, 438, 3594

Dutton A. A., Macciò A. V., Mendel J. T., Simard L., 2013, MNRAS, 432, 2496

Fan L., Lapi A., De Zotti G., Danese L., 2008, ApJ, 689, L101

Fan L., Lapi A., Bressan A., Bernardi M., De Zotti G., Danese L., 2010, ApJ, 718, 1460

Faure C. et al., 2008, ApJS, 176, 19

Faure C. et al., 2011, A&A, 529, A72

Ferreras I., La Barbera F., de la Rosa I. G., Vazdekis A., de Carvalho R. R., Falcón-Barroso J., Ricciardelli E., 2013, MNRAS, 429, L15

Gavazzi R., Treu T., Rhodes J. D., Koopmans L. V. E., Bolton A. S., Burles S., Massey R. J., Moustakas L. A., 2007, ApJ, 667, 176

Gerhard O., Kronawitter A., Saglia R. P., Bender R., 2001, AJ, 121, 1936

Gnedin O. Y., Kravtsov A. V., Klypin A. A., Nagai D., 2004, ApJ, 616, 16

Gnedin O. Y., Weinberg D. H., Pizagno J., Prada F., Rix H.-W., 2007, ApJ, 671, 1115

Goudfrooij P., Kruijssen J. M. D., 2013, ApJ, 762, 107

Goudfrooij P., Kruijssen J. M. D., 2014, ApJ, 780, 43

Graves G. J., Faber S. M., Schiavon R. P., 2009, ApJ, 698, 1590

Grillo C., 2010, ApJ, 722, 779

Grillo C., Gobat R., 2010, MNRAS, 402, L67

Grillo C., Gobat R., Lombardi M., Rosati P., 2009, A&A, 501, 461

Heymans C. et al., 2006, MNRAS, 371, L60

Hilz M., Naab T., Ostriker J. P., 2013, MNRAS, 429, 2924

Hopkins P. F., Hernquist L., Cox T. J., Dutta S. N., Rothberg B., 2008, ApJ, 679, 156

Hopkins P. F., Hernquist L., Cox T. J., Keres D., Wuyts S., 2009, ApJ, 691, 1424

Humphrey P. J., Buote D. A., 2010, MNRAS, 403, 2143

Hyde J. B., Bernardi M., 2009, MNRAS, 396, 1171

Khochfar S., Silk J., 2006, ApJ, 648, L21

Kochanek C. S., 1991, ApJ, 373, 354

Komatsu E. et al., 2011, ApJS, 192, 18

Koopmans L. V. E., Treu T., Bolton A. S., Burles S., Moustakas L. A., 2006, ApJ, 649, 599

La Barbera F., de Carvalho R. R., 2009, ApJ, 699, L76

La Barbera F., de Carvalho R. R., de La Rosa I. G., Lopes P. A. A., Kohl-Moreira J. L., Capelato H. V., 2010, MNRAS, 408, 1313

La Barbera F., Ferreras I., Vazdekis A., de la Rosa I. G., de Carvalho R. R., Trevisan M., Falcón-Barroso J., Ricciardelli E., 2013, MNRAS, 433, 3017

Lagattuta D. J. et al., 2010, ApJ, 716, 1579

Macciò A. V., Dutton A. A., van den Bosch F. C., 2008, MNRAS, 391, 1940

Mandelbaum R., Seljak U., Kauffmann G., Hirata C. M., Brinkmann J., 2006, MNRAS, 368, 715

Marinoni C., Hudson M. J., 2002, ApJ, 569, 101

Moster B. P., Somerville R. S., Maulbetsch C., van den Bosch F. C., Macciò A. V., Naab T., Oser L., 2010, ApJ, 710, 903

Napolitano N. R. et al., 2005, MNRAS, 357, 691

Napolitano N. R., Romanowsky A. J., Tortora C., 2010, MNRAS, 405, 2351

Navarro J. F., Frenk C. S., White S. D. M., 1996, ApJ, 462, 563 (NFW)

Oguri M., Rusu C. E., Falco E. E., 2014, MNRAS, 439, 2494

Padmanabhan N. et al., 2004, New Astron., 9, 329

Prugniel P., Simien F., 1996, A&A, 309, 749

Prugniel P., Simien F., 1997, A&A, 321, 111

Remus R.-S., Burkert A., Dolag K., Johansson P. H., Naab T., Oser L., Thomas J., 2013, ApJ, 766, 71

Roche N., Bernardi M., Hyde J., 2010, MNRAS, 407, 1231

Rudnick G. et al., 2009, ApJ, 700, 1559

Ruff A. J., Gavazzi R., Marshall P. J., Treu T., Auger M. W., Brault F., 2011, ApJ, 727, 96

Rusin D., Kochanek C. S., Keeton C. R., 2003, ApJ, 595, 29

Ruszkowski M., Springel V., 2009, ApJ, 696, 1094

Saglia R. P. et al., 2010, A&A, 524, A6

Salpeter E. E., 1955, ApJ, 121, 161

Schneider A., Smith R. E., Macciò A. V., Moore B., 2012, MNRAS, 424, 684

Shankar F., Bernardi M., 2009, MNRAS, 396, L76

Shankar F., Marulli F., Bernardi M., Dai X., Hyde J. B., Sheth R. K., 2010, MNRAS, 403, 117

Shetty S., Cappellari M., 2014, ApJ, 786, L10

Sonnenfeld A., Treu T., Gavazzi R., Suyu S. H., Marshall P. J., Auger M. W., Nipoti C., 2013, ApJ, 777, 98

Sparks W. B., Jorgensen I., 1993, AJ, 105, 1753

Spiniello C., Koopmans L. V. E., Trager S. C., Czoske O., Treu T., 2011, MNRAS, 417, 3000

Spiniello C., Trager S. C., Koopmans L. V. E., Chen Y. P., 2012, ApJ, 753, L32

Swindle R., Gal R. R., La Barbera F., de Carvalho R. R., 2011, AJ, 142, 118

Thomas J., Saglia R. P., Bender R., Thomas D., Gebhardt K., Magorrian J., Corsini E. M., Wegner G., 2007, MNRAS, 382, 657

Thomas J., Saglia R. P., Bender R., Thomas D., Gebhardt K., Magorrian J., Corsini E. M., Wegner G., 2009, ApJ, 691, 770

Thomas J. et al., 2011, MNRAS, 415, 545

Thomas D. et al., 2013, MNRAS, 431, 1383

Tortora C., Napolitano N. R., Romanowsky A. J., Capaccioli M., Covone G., 2009, MNRAS, 396, 1132 (T+09)

Tortora C., Napolitano N. R., Cardone V. F., Capaccioli M., Jetzer P., Molinaro R., 2010a, MNRAS, 407, 144

Tortora C., Napolitano N. R., Romanowsky A. J., Jetzer P., 2010b, ApJ, 721, L1

Tortora C., La Barbera F., Napolitano N. R., de Carvalho R. R., Romanowsky A. J., 2012, MNRAS, 425, 577

Tortora C., Romanowsky A. J., Napolitano N. R., 2013, ApJ, 765, 8

Tortora C., Romanowsky A. J., Cardone V. F., Napolitano N. R., Jetzer P., 2014, MNRAS, 438, L46

Treu T., Koopmans L. V. E., 2004, ApJ, 611, 739

Treu T., Auger M. W., Koopmans L. V. E., Gavazzi R., Marshall P. J., Bolton A. S., 2010, ApJ, 709, 1195

Trujillo I., Burkert A., Bell E. F., 2004, ApJ, 600, L39

Trujillo I. et al., 2006, ApJ, 650, 18

Trujillo I., Ferreras I., de La Rosa I. G., 2011, MNRAS, 415, 3903
Valentinuzzi T. et al., 2010a, ApJ, 712, 226
Valentinuzzi T. et al., 2010b, ApJ, 721, L19
van den Bosch F. C. et al., 2007, MNRAS, 376, 841
van Dokkum P. G., Franx M., 2001, ApJ, 553, 90
van Dokkum P. G. et al., 2010, ApJ, 709, 1018
Vazdekis A., Ricciardelli E., Cenarro A. J., Rivero-González J. G., Díaz-García L. A., Falcón-Barroso J., 2012, MNRAS, 3156
Vulcani B. et al., 2011, MNRAS, 412, 246
Vulcani B. et al., 2014, MNRAS, 441, 1340

Wegner G. A., Corsini E. M., Thomas J., Saglia R. P., Bender R., Pu S. B., 2012, AJ, 144, 78
Weidner C., Ferreras I., Vazdekis A., La Barbera F., 2013, MNRAS, 435, 2274
White S. D. M. et al., 2005, A&A, 444, 365
Wu X., Gerhard O., Naab T., Oser L., Martinez-Valpuesta I., Hilz M., Churazov E., Lyskova N., 2014, MNRAS, 438, 2701

This paper has been typeset from a TEX/LATEX file prepared by the author.